Available online at www.sciencedirect.com
ScienceDirect
Journal of Power Sources 164 (2007) 315–321
JOURNAL OF POWER SOURCES
www.elsevier.com/locate/jpowsour

Dynamic behavior of PEM fuel cell and microturbine power plants

M.Y. El-Sharkh *, N.S. Sisworahardjo, M. Uzunoglu, O. Onar, M.S. Alam

Department of Electrical and Computer Engineering, University of South Alabama, 307 University Boulevard North, Mobile, AL 36688-0002, USA

Received 6 July 2006; received in revised form 16 August 2006; accepted 15 September 2006
Available online 28 November 2006

Abstract

This paper presents a comparison between the dynamic behavior of a 250 kW stand-alone proton exchange membrane fuel cell power plant (PEM FCPP) and a 250 kW stand-alone microturbine (MT). Dynamic models for the two are introduced. To control the voltage and the power output of the PEM FCPP, voltage and power control loops are added to the model. For the MT, voltage, speed, and power control are used. Dynamic models are used to determine the response of the PEM FCPP and MT to a load step change. Simulation results indicate that the response of the MT to reach a steady state is about twice as fast as the PEM FCPP. For stand-alone operation of a PEM FCPP, a set of batteries or ultracapacitors is needed in order to satisfy the power mismatch during transient periods. Software simulation results are obtained by using MATLAB®, Simulink®, and SimPowerSystems®.

Keywords: Distributed generation; Dynamic model; Microturbine; Proton exchange membrane fuel cell; Simulation

1. Introduction

Distributed generation (DG) is one of the most promising alternatives for generating and delivering electric power. The need for DG is heightened due to the restructuring of the electric power industry and the increase in electric power demand. In addition, the need becomes more acute because of stringent present-day power quality and system reliability requirements. Generally, a DG system consists of small-scale power generators that are located close to load centers. Primary advantages of the DG system are: (a) consumers can generate electric power with or without grid backup; (b) the excess generation can be sold back to the grid at low load conditions. Fuel cells and microturbines as DG sources are among the potential candidates for supplying electric and thermal energy to residential and commercial loads [1].

Fuel cells are not only characterized by higher efficiency than conventional power plants, but they are also environmentally clean, have extremely low emission of oxides of nitrogen and sulfur and have very low noise. The main components of the fuel cell system include the fuel processing unit or the reformer, the fuel cell stack and the power-conditioning unit [2,3]. Reformer produces hydrogen to supply the fuel cell stack by processing any hydrocarbon fuel such as propane, methane, or methanol. Using the hydrogen input and oxygen from air, fuel cell stack produces electricity and water through an electrochemical process. The output from a fuel cell is dc power. To provide power to a residential load, or to the electrical grid, a power-conditioning unit is needed. Many models have been proposed to simulate the fuel cell in the literature [4–8]. Due to the low working temperature (80–100 °C) and fast start up, proton exchange membrane (PEM) fuel cell power plants (FCPPs) are the best candidates for residential and commercial applications. Based on the model introduced in [4,5], a model for a 250 kW PEM FCPP is developed and used to study the dynamic behavior in response to a step change.

Microturbines (MT) are small and simple gas turbines that have three main components: compressor, combustor, and turbine. The high-pressure air from the compressor when mixed with the injected fuel forms a combustible mixture. The mixture is ignited in the combustor to produce hot gas flow, which is used to drive the turbine [9]. Two distinct types of MT are identified in the literature, the single- and split-shaft MT [10]. Single-shaft MT is high speed in nature, where the electric generator and turbine are mounted on the same shaft. Split-shaft MT uses a gearbox to connect the electric generator to the turbine shaft.

* Corresponding author. Tel.: +1 251 461 1562; fax: +1 251 460 6028.
E-mail address: yel-shark@usouthal.edu (M.Y. El-Sharkh).

0378-7753/$ – see front matter © 2006 Elsevier B.V. All rights reserved.
doi:10.1016/j.jpowsour.2006.09.100

Many models are used in the literature to describe the behavior of the MT [10–14]. In this paper, the model used in [11] has been modified by adding speed and voltage control loops.

This paper is organized as follows. Section 2 presents the modified 250 kW PEM FCPP model. Section 3 presents the MT model. Tests and results are discussed in Section 4. Section 5 is the conclusion.

2. PEM fuel cell model

2.1. Model description

In [4,5,15] a model of a PEM FCPP is introduced. In this paper the model has been modified to simulate a 250 kW PEM fuel cell.

The model is based on simulating the relationship between the output voltage and partial pressures of hydrogen, oxygen, and water. A detailed model is shown in Fig. 1, which includes the PEM FCPP, reformer, and power conditioning unit models [4]. The model is verified based on the experimental results obtained using the PEM FCPP, which is currently operated in authors' laboratory. All of the model parameters were tuned to make the model produce similar response as the real system.

The 250 kW PEM FCPP model parameters are based on 440 V dc bus voltage, stack current capacity of 94 A, and cell voltage of 0.8 V. Based on the above figures, the PEM FCPP consists of six parallel stacks, each stack has 550 cells in series. Using the indicated number of cells and stacks the 250 kW PEM FCPP model parameters are given in Table 1, where, E is the Nernst voltage (V), p_{H_2} is the hydrogen partial pressure (atm),

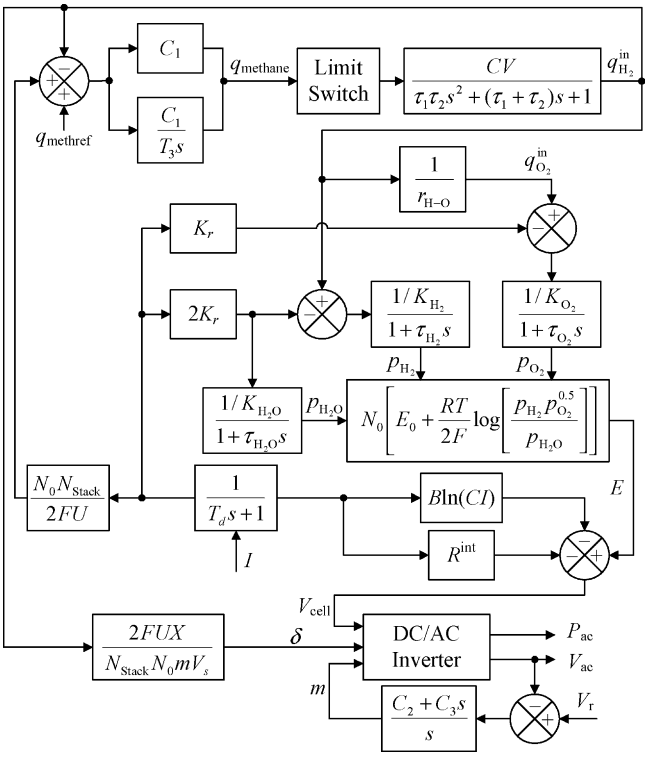

Fig. 1. PEM FCPP system block diagram.

Table 1
PEM FCPP model parameters

Parameter	Value
Stack temperature	343 K
Faraday's constant (F)	96484600 C kmol^{-1}
Universal gas constant (R)	8314.47 J kmol^{-1} K^{-1}
No load voltage (E_0)	0.8 V
Number of cells per stack, N_0	550
Number of stacks, N_{stack}	6
K_r constant = $N_0/(4F)$	1.4251×10^{-6} kmol s^{-1} A^{-1}
Utilization factor (U)	0.8
Hydrogen valve constant (K_{H_2})	4.22×10^{-5} kmol s^{-1} atm^{-1}
Water valve constant (K_{H_2O})	7.716×10^{-6} kmol s^{-1} atm^{-1}
Oxygen valve constant (K_{O_2})	2.11×10^{-5} kmol s^{-1} atm^{-1}
Hydrogen time constant (τ_{H_2})	3.37 s
Water time constant (τ_{H_2O})	18.418 s
Oxygen time constant (τ_{O_2})	6.74 s
Reformer time constant (τ_1)	2 s
Reformer time constant (τ_2)	2 s
Reformer PI gain (C_1)	0.25
Conversion factor (CV)	2
Activation voltage constant (B)	0.04777 A^{-1}
Activation voltage constant (C)	0.0136 V
Internal resistance (R^{int})	0.2778 Ω
External line reactance (X)	0.05 Ω
PI gain constants C_2, C_3	0.1, 10
Voltage reference signal (V_r)	1.0 p.u.
Methane reference signal ($Q_{methref}$)	0.000015 kmol s^{-1}
Hydrogen–oxygen flow ratio (r_{H-O})	1.168
Current delay time constant (T_d)	3 s

p_{H_2O} is the water partial pressure (atm), p_{O_2} is the oxygen partial pressure (atm), $q^{in}_{O_2}$ is the input molar flow of oxygen (kmol s^{-1}), and $q^{in}_{H_2}$ is the hydrogen input flow (kmol s^{-1}).

2.2. FCPP power control

Power control scheme has been developed in [15] that can be summarized as follows:

$$P_{ac} = \frac{m V_{cell} V_s}{X} \sin(\delta) \tag{1}$$

where P_{ac} is the ac power, m the modulation index, V_{cell} dc voltage, V_s the load voltage, X the external line reactance, and δ is phase angle of the ac voltage mV_{cell}.

Assuming a lossless inverter:

$$P_{ac} = P_{dc} = V_{cell} I \tag{2}$$

$$q_{H_2} = \frac{N_{Stack} N_0 I}{2FU} \tag{3}$$

where P_{dc} is the dc power, I the stack current, q_{H_2} input molar flow of hydrogen, N_{Stack} the number of stacks, N_0 the number of cells per stack, F Faraday's constant, and U is utilization factor.

From (1), (2), and (3):

$$\sin(\delta) = \frac{2FUX}{m V_s N_0 N_{Stack}} q_{H_2}. \tag{4}$$

Assuming a small phase angle $\sin(\delta) \cong \delta$,

$$\delta = \frac{2FUX}{mV_s N_0 N_{Stack}} q_{H_2}. \quad (5)$$

Eq. (5) describes the relationship between output voltage phase angle δ and hydrogen flow q_{H_2}. Eqs. (1) and (5) show that the active power as a function of the voltage phase angle δ can be controlled using the amount of hydrogen flow.

Output voltage can be controlled by the modulation index m. The modulation index is controlled using a PI controller. The input to the PI controller is the error signal (difference between ac terminal voltage V_{ac} and reference voltage V_r).

3. Microturbine model

3.1. Model description

As mentioned earlier, microturbines are classified in two categories, the single-shaft or high-speed turbine and split-shaft or low speed turbine. In the single-shaft configuration, the compressor, turbine, and electric generator are mounted on the same shaft. The turbine speed is in the range of 50,000–120,000 rpm. The frequency of the produced voltage will in the range of 1500–4000 Hz. To reduce the frequency to 60 Hz, a cyclo-converter is used. In split-shaft microturbine, the electric generator is driven through a gearbox. The gearbox is used to reduce the speed to 3600 rpm. Assuming a two-pole synchronous generator (SG), the frequency will be 60 Hz. In this case, no power electronic devices are needed for frequency conversion.

In this paper, a split-shaft model is used to determine the dynamic behavior of a microturbine. In [11], the authors used the GAST model without speed control to simulate the split-shaft microturbine. In this paper, due to the use of a SG, a speed controller is developed and used with the GAST model. Using a two-pole SG with a split-shaft microturbine that runs at 3600 rpm, eliminates the need for frequency conversion. The model details and parameters are shown in Fig. 2 and Table 2, respectively. The focus of this paper is on the electro-mechanical behavior of the MT at normal operation condition, where, the load can change gradually, or suddenly. Fast dynamics such as faults, loss of power, and startup and shutdown transients are not considered.

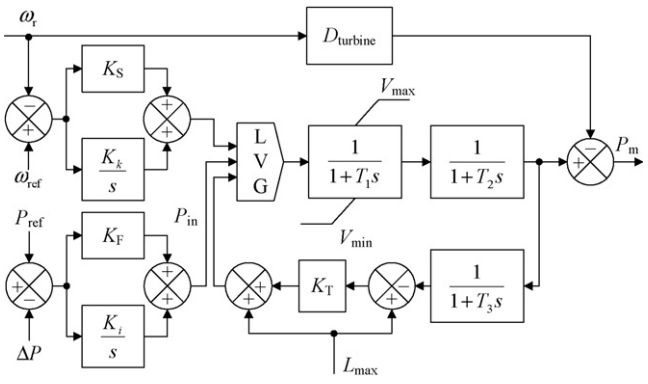

Fig. 2. MT system block diagram with speed and power control.

Table 2
MT model parameters

Parameter	Value
Rated power ($P_{rated\text{-}MT}$)	250 kW
Real power reference (P_{ref})	1.0 p.u.
Damping of turbine ($D_{turbine}$)	0.03
Fuel system lag time constant (T_1)	10.0 s
Fuel system lag time constant (T_2)	0.1 s
Load limit time constant (T_3)	3.0 s
Load limit (L_{max})	1.2
Maximum value position (V_{max})	1.2
Minimum value position (V_{min})	−0.1
Temperature control loop gain (K_T)	1.0
Power control proportional gain (K_F)	0.1
Power control integral gain (K_i)	1.0
Speed control proportional gain (K_S)	1000
Speed control integral gain (K_k)	12.5
Speed reference (ω_{ref})	1.0 p.u.

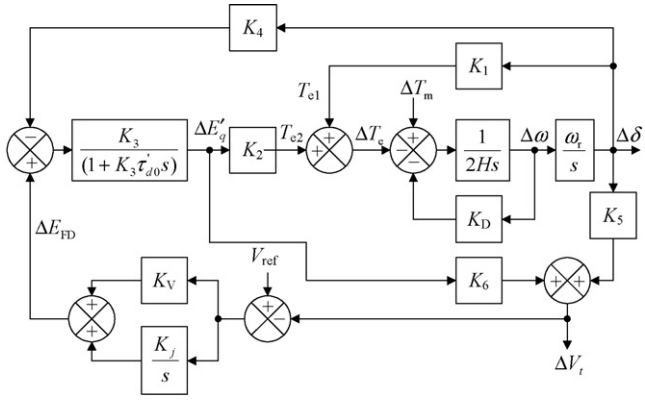

Fig. 3. Synchronous machine block diagram with voltage control.

3.2. Simplified synchronous generator model

A simplified model of a synchronous machine is given in [16]. A modified version of this model is presented in Fig. 3. The equations that are used to drive the synchronous machine model are explained in Appendix A. To simulate the synchronous machine, the authors used a predefined model existing in SimPowerSystems® of the MATLAB® software [17]. The model parameters are as shown in Table 3, where K_V, K_j are the PI gains of the excitation voltage controller (V).

Table 3
Synchronous machine model parameters

Parameter	Value
Rated power ($P_{rated\text{-}SG}$)	250 kW
Rated line to line voltage (V_{rated})	660 V
Frequency (F)	60 Hz
Inertia constant (H)	0.822 s
Damping factor (K_D)	33.63 p.u.
Number of poles (P)	2
Internal resistance (R)	0.02 p.u.
Internal reactance (X)	0.3 p.u.

3.3. MT speed control

As shown in Fig. 2, speed control is achieved by comparing the rotor speed ω_r with a reference speed ω_{ref}. A PI controller is used to control the error signal $(\omega_{ref} - \omega_r)$. The PI controller output is then connected as a low value gate input.

3.4. MT real power control

Referring to Fig. 2, to control the mechanical output power from the microturbine, a PI controller is used. The input to the PI controller is the error signal $(P_{ref} - \Delta P)$, where ΔP is the difference between the generated and the load power.

3.5. MT voltage control

As stated in Table 3, the SG output voltage is 660 V. To compare the SG voltage and the PEM FCPP voltage (440 V) a transformer is used to step down the SG voltage to 440 V at the load terminals. A PI controller is used to control the output voltage by controlling the excitation voltage of the synchronous generator. The input signal to the PI controller is the difference between the output voltage and reference voltage V_{ref}. The parameters for the PI controller are $K_V = 0.005$, and $K_j = 0.1$.

4. Test and results

To test the fuel cell and the microturbine dynamic models, a step change in the load is used as illustrated in Fig. 4. The simulation time is 60 s, the initial load is 80 kW, and increased to 160 kW after 30 s. The effect of stepping the load on the output power of the MT and PEM FCPP are shown in Figs. 5 and 6.

Comparing Figs. 5 and 6, shows that the PEM FCPP took about 10 s to change the output power to match the load level. The delay is mainly caused by the reformer, due to the slow gas processing response. On the other hand, the MT has a much faster response compared to the PEM FCPP. As shown in Fig. 5, the MT response was almost instantaneous, but due to inertia and damping factor of MT and SG, the output power oscillates for about 5 s before it reaches steady state condition. The above comparison showed that the PEM FCPP has poor load following characteristics. Therefore, for stand-alone operation, the PEM FCPP must incorporate a battery or ultracapacitor to satisfy the load requirement during the transient period. Figs. 7 and 8 demonstrate the

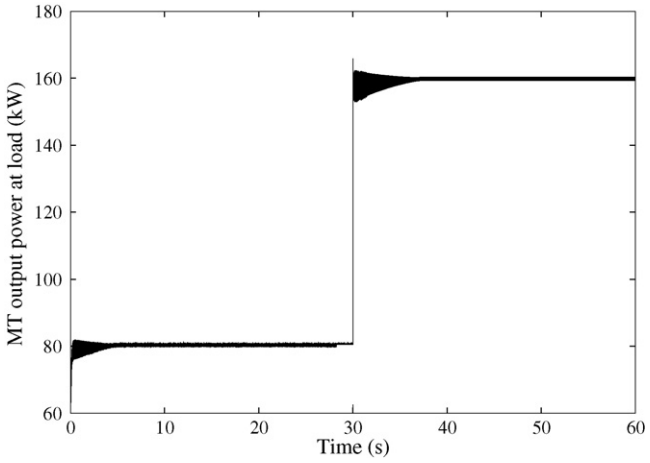

Fig. 5. MT output power.

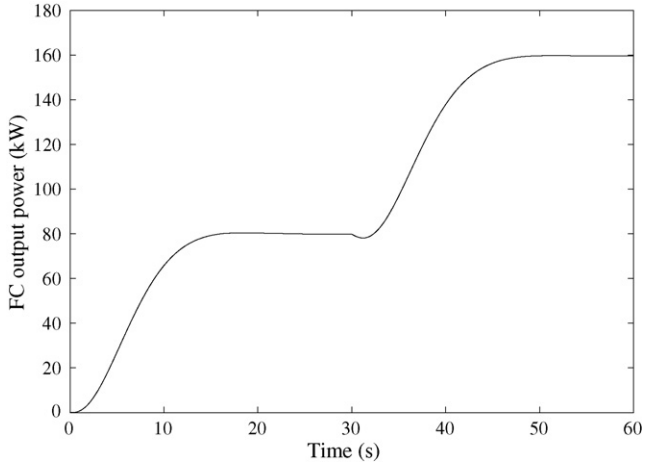

Fig. 6. PEM FCPP output power.

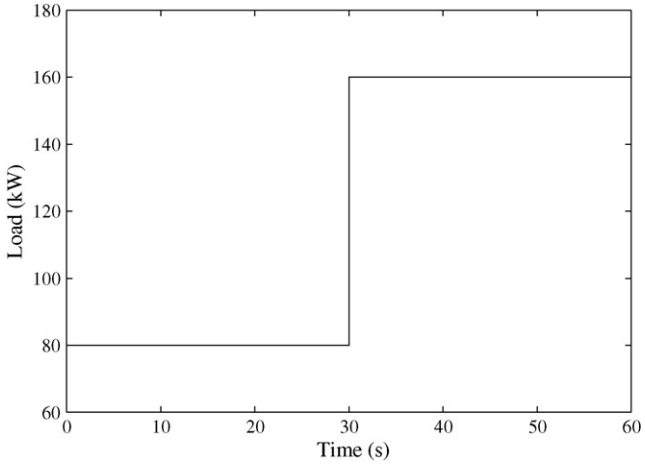

Fig. 4. Step change in load.

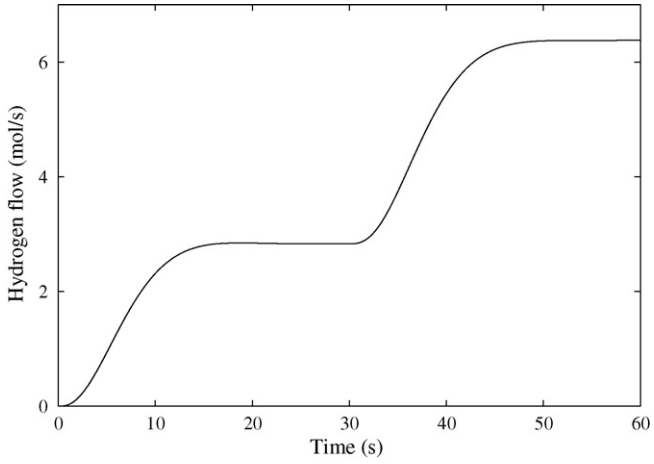

Fig. 7. Hydrogen flow in PEM FCPP.

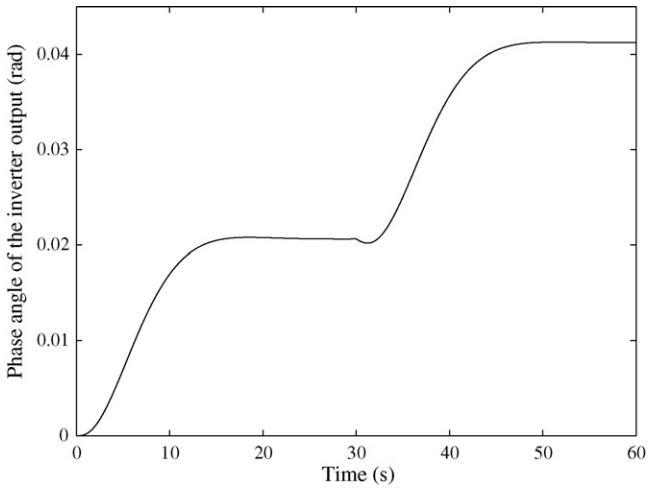

Fig. 8. Inverter phase angle.

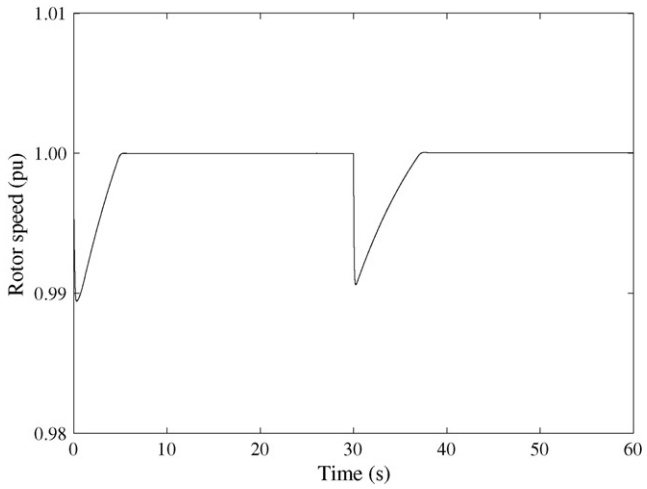

Fig. 10. Synchronous generator rotor speed.

change in hydrogen flow from the reformer to the stack of the PEM FCPP and the phase angle of the inverter.

Despite the fact that the MT response is much faster than that of the PEM FCPP, the mechanical power output from the turbine suffers a time delay of about 5 s as shown in Fig. 9. During this period, the power mismatch is compensated by the rotor inertia, which causes a momentarily reduction in the rotor speed as illustrated in Fig. 10. During the low rotor speed period, the speed controller and the power controller increase the input power to the turbine. When the mechanical input power matches the electrical power output, the speed controller brings the rotor speed back to synchronous speed (Fig. 10).

The change in the MT and the PEM FCPP voltage at the load terminals is demonstrated in Figs. 11 and 12. In Fig. 11, the MT voltage is slightly decreased when the load increases due to voltage drop in the line and transformer. At $t = 30$ s, a very short period voltage dip of 20 V occurs due to the sudden change of the load. As a result of the drop in voltage, the voltage controller increases the excitation level by 2.5% to keep the voltage at the same level of 440 V (Fig. 13).

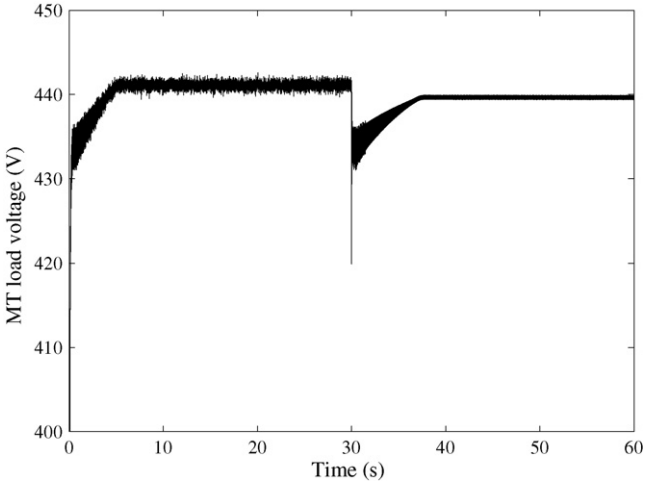

Fig. 11. MT voltage at load terminals.

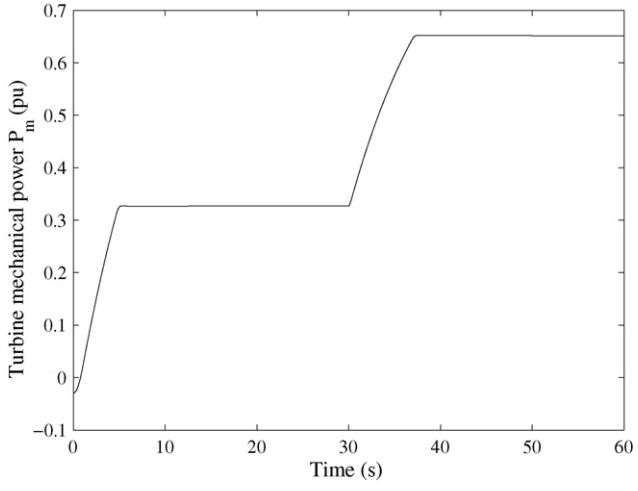

Fig. 9. Turbine mechanical power.

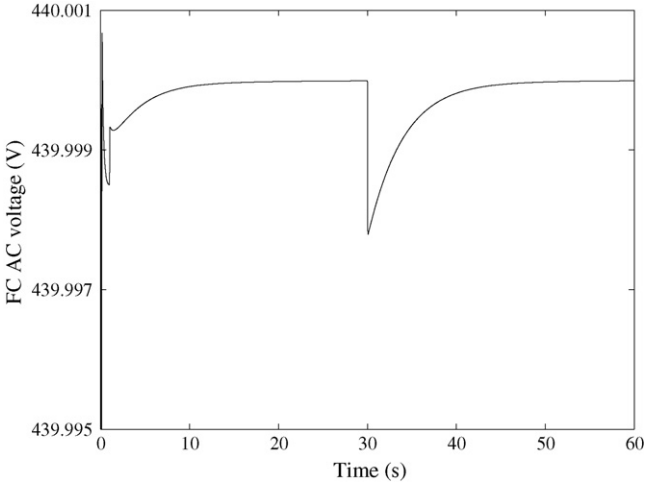

Fig. 12. PEM FCPP voltage at load terminals.

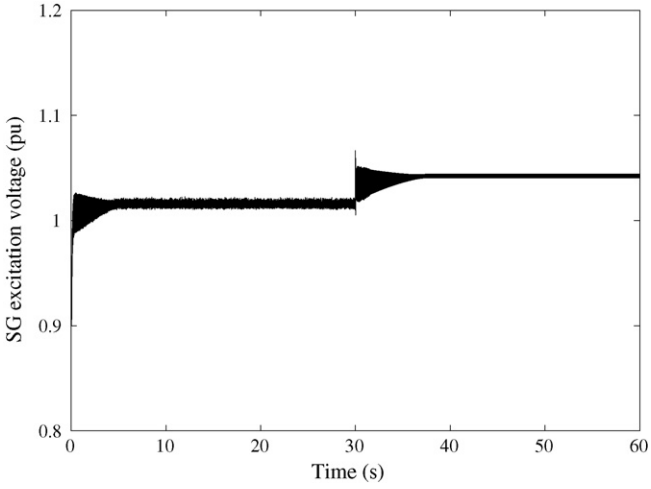

Fig. 13. SG excitation voltage.

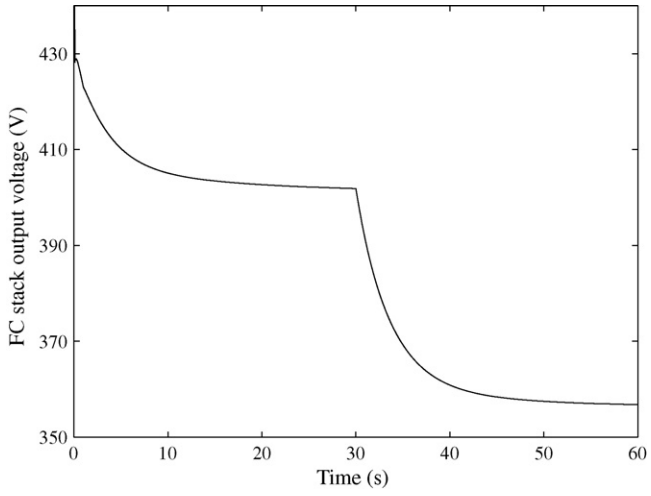

Fig. 14. PEM FCPP stack output voltage.

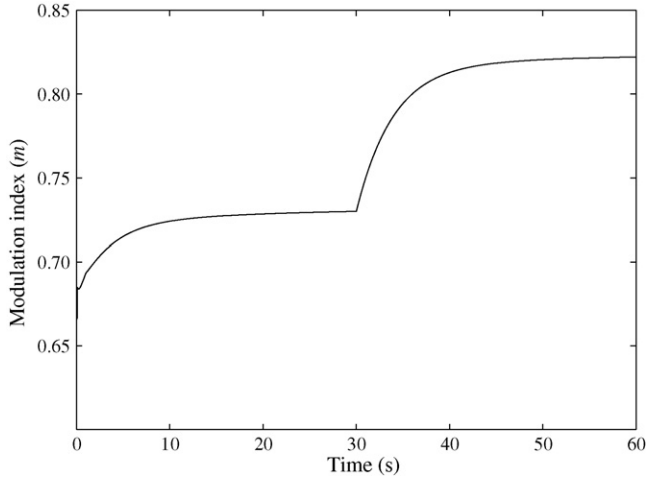

Fig. 15. Inverter modulation index.

Referring to Fig. 12, the change in the PEM FCPP ac voltage is insignificant. This is mainly due to the effectiveness of the PEM FCPP voltage controller (Fig. 1). Fig. 14 shows that the fuel cell stack output voltage of the PEM FCPP decreases by 11.82% as the load doubles. The fuel cell stack output voltage is fed to a dc/dc boost converter having a constant gain 1.5. The change in the modulation index to increase the output voltage is inversely proportional to the voltage decrease as illustrated in Fig. 15.

5. Conclusion

Dynamic behaviors of the PEM FCPP and MT are studied and evaluated. Dynamic models of the 250 kW PEM FCPP and MT with speed and power control are developed. The step load change test results indicate that the response of the MT to reach a steady state is about twice as fast as that of the PEM FCPP. Due to poor load following characteristics of the PEM FCPP, a set of batteries or ultracapacitors are essential in order to satisfy the power mismatch during transient period. Although the MT response has a better load following capability, the mechanical power output experiences a momentary delay. During this delay period, rotor speed decreases as part of the rotor kinetic energy is used to compensate the power mismatch. By the time the MT system reaches a new equilibrium point, the speed control brings the rotor speed back to synchronous speed.

In order to maintain the voltage level of the SG, the voltage controller increases the excitation level by 2.5%. Meanwhile, in the PEM FCPP, the voltage dip is very insignificant. Although its dc output voltage decreases by 11.82%, the change of modulation index maintains a constant ac voltage level.

Appendix A

Synchronous machine model as explained in [16] is constructed based on synchronous machine swing equation. Swing equation for power system dynamics can be expressed in many forms. Given ω in electrical deg s^{-1}, swing equation is expressed as:

$$\frac{\pi H}{90}\frac{d\omega}{dt} = T_m - T_e = T_a. \tag{A.1}$$

Linearizing the swing Eq. (A.1) results in an equation as shown in (A.2).

$$\tau_j \Delta\omega s = \Delta T_m - \Delta T_e \tag{A.2}$$

The basic equations for the simplified linear synchronous generator model consist of three equations, i.e.,

$$\Delta E'_q = \frac{K_3}{1 + K_3\tau'_{d0}s}\Delta E_{FD} - \frac{K_3 K_4}{1 + K_3\tau'_{d0}s}\Delta\delta \tag{A.3}$$

$$\Delta T_e = K_1\,\Delta\delta + K_2\,\Delta E'_q \tag{A.4}$$

$$\Delta V_t = K_5\,\Delta\delta + K_6\,\Delta E'_q. \tag{A.5}$$

The constants K_1, K_2, K_3, K_4, K_5, and K_6 are dependent upon the network parameters, the quiescent operating conditions, and the infinite bus voltage.

The simplified synchronous generation model as presented in Fig. 3 is obtained by combining the effect of the damping torque with voltage control, and Eqs. (A.2)–(A.5). The variables are defined as follows:

T_m	mechanical torque
T_a	accelerating torque
T_e	electromagnetic torque
τ_j	time constant ($\tau_j = 2H/\omega_r$)
τ'_{d0}	*d*-axis transient open circuit time constant
δ	rotor angle
V_t	terminal voltage
E'_q	rms of the peak stator voltage
E_{FD}	stator EMF
ω_r	rotor angular speed
K_1	change in the electrical torque for small change in rotor angle at constant *d*-axis flux linkage
K_2	change in the electrical torque for small change in the *d*-axis flux linkage at constant rotor angle
K_3	impedance factor
K_4	constant related to demagnetizing effect
K_5	change in the terminal voltage V_t for a small change in rotor angle at constant d-axis flux linkage
K_6	change in the terminal voltage V_t for a small change in the *d*-axis flux linkage at constant rotor angle
K_D	damping constant
H	inertia constant.

References

[1] T. Moore, Market potential high for fuel cells, EPRI J. 22 (3) (1997) 6–17.

[2] J.E. Larmine, A. Dicks, Fuel Cell Systems Explained, second ed., John Wiley and Sons, 2000.

[3] W. Vielstich, A. Lamm, H. Gasteiger, Handbook of Fuel Cells: Fundamentals, Technology Applications, vol. 4, John Wiley and Sons, May 2003.

[4] M.Y. El-Sharkh, A. Rahman, M.S. Alam, P.C. Byrne, A.A. Sakla, T. Thomas, J. Power Sources 138 (1–2) (2004) 199–200.

[5] M. Uzunoglu, M.S. Alam, Dynamic modeling, design, and simulation of a combined PEM fuel cell and ultracapacitor system for stand-alone residential applications, IEEE Trans. on Energy Conv. 21 (3) (2006) 767–775.

[6] J.C. Amphlett, R.F. Mann, B.A. Peppley, P.R. Roberge, A. Rodrigues, J. Power Sources 61 (1996) 183–188.

[7] J. Padulles, G.W. Ault, J.R. McDonald, J. Power Sources 86 (2000) 495–500.

[8] J.C. Amphlett, R.M. Baumert, R.F. Mann, B.A. Peppley, P.R. Roberge, A. Rodrigues, J. Power Sources 49 (1994) 349–356.

[9] W.I. Rowen, Trans. ASME 105 (1) (1983) 865–869.

[10] G.N. Kariniotakis, N.L. Soultanis, A.I. Tsouchnikas, S.A. Papathanasiou, N.D. Hatziargyriou, Dynamic modeling of microgrids, in: Proceedings of Future Power Systems Conference 2005, Amsterdam, November 2005, pp. 1–7.

[11] Y. Zhu, K. Tomsovic, Electric Power Syst. Res. 62 (1) (2002) 1–11.

[12] F. Jurado, Energy Conv. Manage. 46 (3) (2005) 385–401.

[13] M. Nagpal, A. Moshref, G.K. Morison, P. Kundur, Experience with testing and modeling of gas turbine, in: Proceedings of the IEEE/PES 2001 Winter Meeting, Columbus, Ohio, USA, January/February 2001, 2001, pp. 652–656.

[14] S.R. Guda, Modeling and power management of a hybrid wind microturbine power generation system, M.S. Thesis, Dept. Electrical Eng., Montana State University, Bozeman, Montana.

[15] M.Y. El-Sharkh, A. Rahman, M.S. Alam, P.C. Byrne, A.A. Sakla, T. Thomas, IEEE Trans. Power Syst. 19 (4) (2004) 2022–2028.

[16] P.M. Anderson, A.A. Fouad, Power System Control and Stability, vol. 1, The Iowa State University Press, 1977.

[17] SimPowerSystems User's Guide, ver. 4, The MathWorks, Inc., 2006.